Journal of Stress Analysis
Vol. 9, No. 1, 2025, 9-25
Bu-Ali Sina University

ORIGINAL RESEARCH PAPER

Nonlinear Axisymmetric Forced Vibrations of CNT-Reinforced FGM Plate with Elastic Boundary Conditions Using Multiple Scales Method

Reza Azarafza[a,*], **Ali Davar**[b]

[a] Faculty of Material, Manufacturing Technologies, Malek Ashtar University of Technology, Tehran, Iran.
[b] Composite Research Center, Malek Ashtar University of Technology, Tehran, Iran.

Article info

Article history:
Received 13 July 2024
Received in revised form
01 June 2025
Accepted 15 June 2025

Keywords:
Nonlinear axisymmetric forced vibrations
Annular plate
Functionally graded carbon nanotubes
Eastic boundary conditions
Multiple time-scales method

Abstract

Nonlinear axisymmetric forced vibrations of annular circular plates reinforced by functionally graded carbon nanotubes (FG-CNTs) under elastic boundary conditions and harmonic pressure are studied in this paper. The material properties of the plate are assumed to be graded according to the different types of distribution patterns along the plate thickness. Using Hamilton's principle and Von Karman's nonlinear strain-displacement relations, partial differential equations of motion are derived. In the first step, the linear equations of the system are using the generalized differential quadratic method (GDQM), and the linear natural frequencies and mode shapes of the plate are obtained. In the second step, after applying the Galerkin method, the nonlinear partial differential equations of the plate are converted into nonlinear ordinary differential equations. Afterward, in order to acquire the nonlinear frequencies of the plate, the nonlinear equations of the plate are solved analytically using the multiple time-scales method. Finally, the effects of some system parameters, such as the volume fraction and distribution pattern of the CNTs, the aspect ratios of the plate, the boundary conditions and the elastic foundation on the nonlinear frequency response and time history of the plate are studied. In order to validate the outcomes, the presented results are compared with those obtained by the previously published papers as well as ABAQUS software.

Nomenclature

K_w	Winkler foundations	ψ	Out-of-plane rotation
K_p	Foundations pasternak	σ_{ii}	Normal stresses
R_i	Inner radius	ε_{ii}	Normal stresses
R_o	outer radius	τ_{ij}	Shear stresses
h	Uniform thickness	γ_{ij}	Shear stresses
K_{R_1}	Rotational springs in outer radius	K_{R_2}	Rotational springs in inner radius
K_{T_1}	Translational springs in outer radius	K_{T_2}	Translational springs in inner radius
V	The work done by applied forces	q	Harmonic pressure
U	Strain energy	K	kinetic energy

*Corresponding author: R. Azarafza (Associate Professor)
E-mail address: azarkntu@yahoo.com
10.22084/jrstan.2025.29427.1257
ISSN: 2588-2597

G^m	Shear modulus of matrix	N	Number of discrete points
η_j	Efficiency parameters	$f(x_j)$	Value of a function
ν^m	Poisson's ratio of Matrix	F	Amplitude of the excitation
ρ^{CNT}	Ddensity of CNT	Ω	Frequency of the excitation
ρ^m	Density of Matrix	T_n	Independent time variables
Λ_{CNT}	Mass fraction of CNT	ω_L	Linear frequency
G_{12}^{CNT}	Shear modulus of CNT	ω_L	Nonlinear frequency
ν_{12}^{CNT}	Poisson's ratio of CNT	E^m	Young's modulus of matrix
r, θ, z	cylindrical coordinates system	u_0, w_0	Displacement components of the mid-plane
E_{11}^{CNT}, E_{22}^{CNT}	Young's modulus of CNT	Q_{ij} $(i,j$ =1,2,5)	Elastic stiffness coefficients
(N_{rr}, $N_{\theta\theta}$, $N_{r\theta}$)	Force resultant	(M_{rr}, $M_{\theta\theta}$, $M_{r\theta}$)	Resultant moments
A_{ij}, B_{ij}, D_{ij}	Stiffness elements	$\overline{W(\tau)}$, $\overline{U(\tau)}$, $\overline{\Psi(\tau)}$	Dimensionless time response along the z, r, and axis

1. Literature Review

Much work has been done nonlinear axisymmetric forced vibrations in the past, which will be discussed below. Mahesh and Harursampath [1] studied the finite-element formulation based on higher order shear deformation theory (HSDT) proposed to evaluate the nonlinear frequency characteristics of the carbon nanotube reinforced magneto-electro-elastic (CNTMEE) plates. The von Kármán type of nonlinear strain–displacement relations was assumed. The nonlinear fundamental frequencies for a given maximum transverse deflection were obtained through direct iterative method. Kuriakose et al. [2] performed comparison studies for the vibration behavior of flax fiber reinforced composite cantilevered plates at different aspect ratios. Studies with aspect ratio variations were performed and the effect of CNT fillers on the vibration characteristics of the NFC flat plates was presented. Their work is significant due to the increasing use of NFCs given the universal drive towards a better sustainable future. Kumar and Kumar [3] presented a free vibration analysis of multiscale functionally graded plates, reinforced with a carbon nanotube. The modified third-order shear deformation theory with a variation in transverse displacement was employed in their work. MATLAB code was developed for C_0 finite element (FE) formulation. Sharma et al. [4] investigated the buckling and free vibration characteristics of functionally graded carbon nanotubes (FG CNT) reinforced plates in the framework of inverse hyperbolic shear deformation theory (IHSDT). The FG CNT material constitutes PmPV matrix and single walled carbon nanotubes (SWCNT) reinforcement. Furthermore, the material properties of the constituents (PmPV matrix and SWCNT) were assumed to be temperature dependent. Zhang and Liu [5] investigated the nonlinear vibration response of a functionally graded carbon nanotube (CNT)-reinforced composite conical shell subjected to external excitation by a stress function method, and the motion state of the conical shell was revealed. Also, the motion equations of the conical shell are derived in the frame of the Hamilton's principle and the Von Kármán nonlinearity. Afshari and Amirabadi [6] conducted a comprehensive study on the free vibration analysis of rotating truncated conical shells reinforced with functionally graded agglomerated carbon nanotubes. The shell was modeled based on the first-order shear deformation theory, and effective mechanical properties were calculated based on the Eshelby–Mori–Tanaka scheme along with the rule of mixtures.

Sun et al. [7] carried out a nonlinear vibration analysis of carbon-nanotube reinforced functionally graded composite (FG-CNTRC) cylindrical shells resting on elastic foundations. Four carbon-nanotube distribution types, namely UD, FGV, FG, and FGX, were considered and the elastic foundation was described using the Pasternak model. According to the first-order shear deformation shell theory, the nonlinear governing equations of the FG-CNTRC cylindrical shells were derived from Lagrange's equations. Ansari et al. [8] investigated the axisymmetric the nonlinear vibration analysis of sandwich annular plates with FG-CNTRC face sheets based on the higher-order shear deformation plate theory. After validating the results of the proposed approach, detailed numerical results are given to analyze the effects of geometrical and material parameters on the nonlinear vibration of FG-CNTRC sandwich annular plates. Uspensky et al. [9] analyzed dynamic instability of a functionally graded carbon nanotube-(CNTs)-reinforced composite joined conical-cylindrical shell in supersonic flow numerically. The higher-order shear deformation theory was applied to

describe the stress–strain state of the thin-walled structure. Avey et al. [10] presented the solution of the nonlinear free vibration problem of composite shell structures containing carbon nanotubes (CNTs) resting on the elastic soils within shear deformation theory (ST). Hashemi et al. [11] investigated the nonlinear free vibration analysis of in-plane bi-directional functionally graded (IBFG) rectangular plates with porosities resting on Winkler–Pasternak elastic foundations. Equations of motion were developed by means of Hamilton's principle and Von Kármán nonlinear strain–displacement relations were based on classical plate theory (CPT). Afterward, the time-dependent nonlinear equations were derived by applying the Galerkin procedure. Hashemi and Jafari [12] conducted a nonlinear free vibrations analysis of the functionally graded (FG) rectangular plate with fully simply supported boundary conditions analytically using modified Lindstedt–Poincare (MLP) method for the first time. For this purpose, with the aid of Von Kármán nonlinear strain-displacement relations, the partial differential equations of motion were developed based on the first-order shear deformation theory (FSDT). Qin et al. [13] presented a unified Fourier series solution to solve the vibration problem of the functionally graded carbon nanotube-reinforcement composite (FG-CNTRC) cylindrical shells, conical shells and annular plates subjected to general boundary conditions, so as to enrich the existing research results on FG-CNTRC structures. The first-order shear deformation theory (FSDT) and the virtual boundary method were employed to derive the energy expressions of FG-CNTRC structures. Ansari et al. [14] carried out a free vibration analysis of embedded functionally graded carbon nanotube-reinforced composite (FG-CNTRC) conical and cylindrical shells as well as annular plates using the variational differential quadrature (VDQ) method. Pasternak-type elastic foundation was taken into consideration. Zhang et al. [15] explored the element-free IMLS-Ritz method to compute the vibration solution of thick functionally graded carbon nanotube-reinforced composite (FG-CNTRC) plates resting on elastic foundations. Also, the vibration frequencies and mode shapes of the FG-CNTRC plates on different Winkler foundations were presented. Stephan et al. [16] presented a novel formulation for inverse finite elastostatics involving elastic bed support along the external boundary (elastic bed boundary condition), replacing the classical Dirichlet boundary condition. An unfitted strategy to compute the solution of the mechanical problem was devised, using in the Immersed Boundary (IB) framework and level sets to describe the geometry. Togun and Bağdatl [17] applied the non-local Euler-Bernoulli beam theory in the nonlinear free and forced vibration analysis of a nanobeam resting on an elastic foundation of the Pasternak type. The analysis considered the small-scale effects of on the frequency. By utilizing Hamilton's principle, the nonlinear equations of motion, accounting for the stretching of the neutral axis, were derived. Li et al. [18] investigated the nonlinear vibration and dynamic buckling of a graphene platelet reinforced sandwich functionally graded porous (GPL-SFGP) plate. The investigated GPL-SFGP plate consists of two metal face layers and a functionally graded porous core reinforced with graphene platelets. The effects of the Winkler–Pasternak elastic foundation, thermal environment, and damping were incorporated into the analysis. Parida and Mohanty [19] studied the nonlinear vibration behavior of a functionally graded plate resting on Pasternak elastic foundation within a thermal environment. A mathematical model was developed based on a higher-order shear deformation theory using Green-Lagrange type nonlinearity. The model includes all the nonlinear terms to obtain a general form and to present the original flexure of the plate. Shahsavari and Boutorabi [20] investigated the damped free and forced vibrations of single-walled piezoelectric carbon nanotubes under longitudinal magnetic field due to surface effects surrounded on a non-linear viscoelastic medium using the nonlocal Euler-Bernoulli beam theory and multiple time scales method. They investigated the effect of hardness-linear damping parameters of the considered nonlinear viscoelastic foundation, applied magnetic field, and base modes for different forms considering surface effects. Sobamowo et al. [21] studied the nonlinear vibrations of single- and double-walled carbon nanotubes resting on a two-parameter foundation in a thermal and magnetic environment using nonlocal elasticity theory. Azhdarzadeh et al. [22] investigated the nonlinear and nonlocal thermo-elastic behavior of a microtube reinforced by functionally distributed carbon nanotubes, with internal and external piezoelectric layers, in the presence of the nonlinear viscoelastic-Hetenyi foundation, and axial fluid flow inside the microtube. Hojat and Taghizadeh [23] investigated the nonlinear dynamics of functionally graded porous annular plates under varying time-dependent loads. Both simply supported and fully clamped boundary conditions were taken into account. The mechanical properties of the functionally graded plate along its thickness were considered according to a modified distribution law. Ma et al. [24] studied the nonlinear subharmonic resonance behavior of an orthotropic rectangular laminated composite plate. The nonlinear dynamic equations of the plate were derived using the theory of high-order shear laminates, Von Karman/s geometric relation for the large deformation of plates, and Hamilton/s principle. Allahverdizadeh et al. [25] developed a semi-analytical approach for the nonlinear free and forced axisymmetric vibration of a thin circular functionally graded plate. The results showed that the free vibration frequencies are dependent on the vibration amplitudes, and that the volume fraction index

has a significant influence on the nonlinear response characteristics of the plate. Shadmani et al. [26] analyzed the nonlinear dynamic response of the truncated conical shells reinforced with carbon nanotubes in a functionally graded ceramic-metal matrix subjected to harmonic excitation. The carbon nanotubes were distributed in three different patterns along the length and thickness of the conical shell.

In this paper, the nonlinear forced vibrations of annular plates reinforced by FG-CNTs with elastic boundary conditions under harmonic loading and half-sine pulse excitation are studied, which has not been observed in previous studies. With the help of FSDT, the equations of plate motion were derived using Von Kármán 's nonlinear strain–displacement relations and Hamilton's principle. Then, the system equations were studied using the GDQM and the natural frequencies and mode shapes of the plate were calculated. Secondly, by applying the Galerkin method, the nonlinear PDEs of the plate were converted into time-dependent nonlinear ODEs. Subsequently, the frequency response of the plate was obtained using the method of multiple time scales. The dynamic time response of the plate was then calculated using the Adams-Bashforth numerical method [26]. Finally, the effects of geometrical and physical parameters on the frequency response, time history, and phase-plane behavior of the plate were examined.

2. Governing Equations

As shown in Figs. 1 (a,b), consider an FG-CNT annular circular plate resting on Winkler (Kw) and Pasternak (Kp) elastic foundations with inner radius R_i, outer radius R_o and uniform thickness h. The distribution of the CNTs in the plate is assumed to be graded along the plate thickness. The origin of the cylindrical coordinate system (r, θ, z) is placed at the center of the plate to define the plate geometry and displacements. As illustrated in this figure, the edges of the plate are elastically constrained, in which the rotational springs are represented by K_{R_1} and K_{R_2}, respectively, at the outer and inner radius, and the translational springs are denoted by K_{T_1} and K_{T_2}, respectively, at the outer and inner radius.

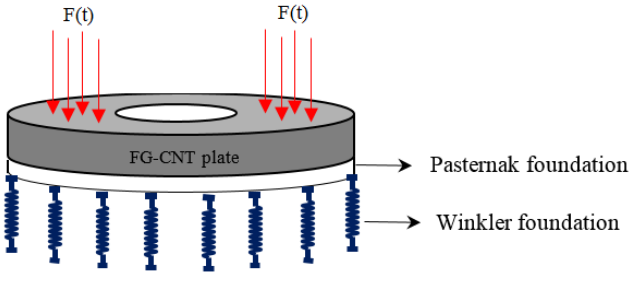

(a)

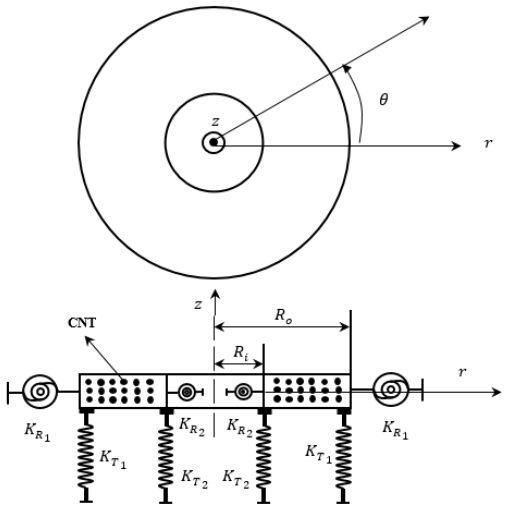

(b)

Fig. 1. Schematic of an FG-CNT annular circular plate with elastic boundaries a) 3D view b) 2D view.

The composite plate consists of matrix (homogeneous phase) reinforced with single-walled CNTs. It should be noted that in this study, five different types of functions are considered for the CNTs distribution along the plate thickness. The mechanical properties of the FG-CNT plate are as follows [27]:

$$E_{11}(z) = \eta_1 V_{CNT}(z) E_{11}^{CNT} + V_m(z) E^m \tag{1}$$

$$\frac{\eta_2}{E_{22}(z)} = \frac{V_{CNT}(z)}{E_{22}^{CNT}} + \frac{V_m(z)}{E^m} \tag{2}$$

$$\frac{\eta_3}{G_{12}(z)} = \frac{V_{CNT}}{G_{12}^{CNT}} + \frac{V_m}{G^m} \tag{3}$$

$$\nu_{12}(z) = V_{CNT}(z)\nu_{12}^{CNT} + V_m(z)\nu^m \tag{4}$$

$$\nu_{21}(z) = \frac{\nu_{12}(z)}{E_{11}(z)} E_{22}(z) \tag{5}$$

$$\rho(z) = V_{CNT}(z)\,\rho^{CNT} + V_m(z)\,\rho^m \tag{6}$$

$$V_{CNT}(z) + V_m(z) = 1 \tag{7}$$

In the above equations, E_{11}^{CNT}, E_{22}^{CNT}, G_{12}^{CNT}, E^m and G^m represent the Young's modulus and shear modulus with the superscripts denoting CNT for reinforcements and m for matrix, respectively, $\eta_j = 1.2.3$ are the efficiency factors, ν_{12}^{CNT} and ν^m are the Poisson's ratio, and $\rho^{CNT}$and ρ^m are the density of CNT and matrix, respectively.

As given in Fig. 2, five different distribution types for CNTs are considered: (I) UD type; (II) FGA, (III) FGV, (IV) FGO and (V) FGX, and the corresponding V_{CNT} for different types of CNTs distribution are expressed as:

$$\begin{aligned} UD &: V_{cnt} = V_{CNT}^* \\ FGA &: V_{cnt}(z) = \left(1 - \frac{2z}{h}\right) V_{CNT}^* \\ FGV &: V_{cnt}(z) = \left(1 + \frac{2z}{h}\right) V_{CNT}^* \end{aligned} \tag{8}$$

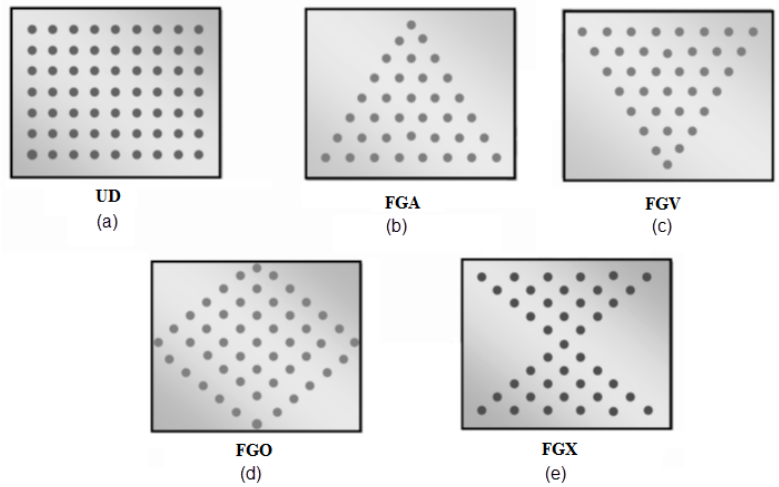

Fig. 2. Distribution pattern of the single-walled CNTs along the plate thickness a) UD b) FGA c) FGV d) FGO e) FGX.

$$FGO: V_{cnt} = 2V^*_{CNT}\left(1 - \frac{|z|}{h}\right)$$
$$FGX: V_{cnt} = 2V^*_{CNT}\left(\frac{|z|}{h}\right)$$

In which V^*_{CNT} is [27]:

$$V^*_{CNT} = \frac{\Lambda_{CNT}}{\Lambda_{CNT} + \left(\frac{\rho_{CNT}}{\rho_m}\right) - \left(\frac{\rho_{CNT}}{\rho_m}\right)\Lambda_{CNT}} \tag{9}$$

In Eq. (9) Λ_{CNT} represents the mass fraction of CNTs.

The displacements of an arbitrary point, according to FSDT are expressed as [28]:

$$\begin{aligned} u\,(r.z.t) &= u_0\,(r.t) + z\psi(r,t) \\ v\,(r.z.t) &= 0 \\ w\,(r.z.t) &= w_0\,(r.t) \end{aligned} \tag{10}$$

where u_0 and w_0 are the displacement components of the mid-plane in radial and transverse displacements, respectively. ψ is the out-of-plane rotation about the θ-axis. The nonlinear strain-displacement relations based on Von Kármán assumptions are given as follows [28]:

$$\begin{aligned} e_{rr} &= \frac{\partial u_0}{\partial r} + \frac{1}{2}\left(\frac{\partial w_0}{\partial r}\right)^2 + z\frac{\partial \psi}{\partial r} \\ e_{\theta\theta} &= \frac{u_0}{r} + \frac{z}{r}\psi \\ \gamma_{rz} &= \frac{\partial w_0}{\partial r} + \psi \end{aligned} \tag{11}$$

The stress-strain relations for an orthotropic material reinforced with CNTs are written as [28]:

$$\begin{pmatrix} \sigma_{rr} \\ \sigma_{\theta\theta} \\ \tau_{rz} \end{pmatrix} = \begin{pmatrix} Q_{11}(z) & Q_{12}(z) & 0 \\ Q_{21}(z) & Q_{22}(z) & 0 \\ 0 & 0 & Q_{55}(z) \end{pmatrix} \begin{pmatrix} \varepsilon_{rr} \\ \varepsilon_{\theta\theta} \\ \gamma_{rz} \end{pmatrix} \tag{12}$$

where σ and ε are the normal stresses and strains, respectively, and τ and γ denote the shear stresses and strains, respectively. Also, the elastic stiffness coefficients Q_{ij} *(i,j=1,2,5)* are calculated from:

$$\begin{aligned} Q_{11} &= \frac{E_{11}}{1 - v_{12}v_{21}}, \\ Q_{22} &= \frac{E_{22}}{1 - v_{12}v_{21}}, \\ Q_{12} &= \frac{v_{21}E_{11}}{1 - v_{12}v_{21}}, \\ Q_{55} &= G_{13} \end{aligned} \tag{13}$$

According to Eqs. (11) and (12), U the strain energy, K the kinetic energy and V the work done by applied forces of the annular circular plate are given, respectively, as follows:

$$\begin{aligned} U &= \frac{1}{2}\int_A \int_{-\frac{h}{2}}^{+\frac{h}{2}} \left(\sigma_{rr}\varepsilon_{rr} + \sigma_{\theta\theta}\varepsilon_{\theta\theta} + \sigma_{rz}\gamma_{rz}\right) dzdA \\ &\quad + \frac{1}{2}\int_A \left(K_w w_0^2 + K_p\left(\frac{\partial w_0}{\partial r}\right)^2\right) dA \\ &= \frac{1}{2}\int_A \left(N_{rr}\left(\frac{\partial u_0}{\partial r} + \frac{1}{2}\left(\frac{\partial w_0}{\partial r}\right)^2\right) + M_{rr}\frac{\partial \psi}{\partial r}\right. \\ &\quad + N_{\theta\theta}\frac{u_0}{r} + M_{\theta\theta}\frac{\psi}{r} + N_{rz}\left(\frac{\partial w_0}{\partial r} + \psi\right) \\ &\quad \left. + K_w w_0^2 + K_p\left(\frac{\partial w_0}{\partial r}\right)^2\right) dA \end{aligned} \tag{14}$$

$$K = \frac{1}{2}\int_A \int_{-\frac{h}{2}}^{+\frac{h}{2}} \rho(z)\left(\dot{u}^2 + \dot{w}^2\right) dz dA$$
$$= \frac{1}{2}\int_A \left(I_0\dot{u}_0^2 + I_2\dot{\psi}^2 + I_0\dot{w}_0^2\right) dA \qquad (15)$$
$$V = \int_A q\ w_0\ dA \qquad (16)$$

where q is harmonic pressure applied to the plate. The force resultant $(N_{rr}, N_{\theta\theta}, N_{r\theta})$, resultant moments $(M_{rr}, M_{\theta\theta}, M_{r\theta})$ and the inertia related terms (I_o, I_2) are written as follows:

$$\left\{\begin{array}{c} N_{rr} \\ N_{\theta\theta} \\ N_{rz} \end{array}\right\} = \int_{-\frac{h}{2}}^{+\frac{h}{2}} \left\{\begin{array}{c} \sigma_{rr} \\ \sigma_{\theta\theta} \\ \tau_{rz} \end{array}\right\} dz$$
$$= \left[\begin{array}{ccc} A_{11} & A_{12} & 0 \\ A_{12} & A_{22} & 0 \\ 0 & 0 & A_{55} \end{array}\right] \left\{\begin{array}{c} \frac{\partial u_0}{\partial r} + \frac{1}{2}\left(\frac{\partial w_0}{\partial r}\right)^2 \\ \frac{u_0}{r} \\ \frac{\partial w_0}{\partial r} + \psi \end{array}\right\}$$
$$+ \left[\begin{array}{cc} B_{11} & B_{12} \\ B_{12} & B_{22} \end{array}\right] \left\{\begin{array}{c} \frac{\partial \psi}{\partial r} \\ \frac{\psi}{r} \end{array}\right\}$$
$$\left\{\begin{array}{c} M_{rr} \\ M_{\theta\theta} \end{array}\right\} = \int_{-\frac{h}{2}}^{+\frac{h}{2}} \left\{\begin{array}{c} \sigma_{rr} \\ \sigma_{\theta\theta} \end{array}\right\} z dz$$
$$= \left[\begin{array}{cc} B_{11} & B_{12} \\ B_{12} & B_{22} \end{array}\right] \left\{\begin{array}{c} \frac{\partial u_0}{\partial r} + \frac{1}{2}\left(\frac{\partial w_0}{\partial r}\right)^2 \\ \frac{u_0}{r} \end{array}\right\}$$
$$+ \left[\begin{array}{cc} D_{11} & D_{12} \\ D_{12} & D_{22} \end{array}\right] \left\{\begin{array}{c} \frac{\partial \psi}{\partial r} \\ \frac{\psi}{r} \end{array}\right\}$$
$$\left\{\begin{array}{c} I_0 \\ I_2 \end{array}\right\} = \int_{-\frac{h}{2}}^{+\frac{h}{2}} \rho(z) \left\{\begin{array}{c} 1 \\ z^2 \end{array}\right\} dz \qquad (17)$$

In which stiffness elements A_{ij}, B_{ij}, and D_{ij} are defined as:

$$\left\{\begin{array}{c} A_{ij} \\ B_{ij} \\ D_{ij} \end{array}\right\} = \int_{-\frac{h}{2}}^{+\frac{h}{2}} \left\{\begin{array}{c} 1 \\ z \\ z^2 \end{array}\right\} Q_{ij}(z)\ dz, \qquad i,j = 1.2$$
$$A_{55} = \kappa \int_{-\frac{h}{2}}^{+\frac{h}{2}} Q_{55} dz, \qquad \kappa = \frac{5}{6}\ \ or\ \ \frac{p^2}{12} \qquad (18)$$

where κ is the shear correction factor. Variation of Eqs. (14)-(16) is:

$$\delta U = \int_A \int_{-\frac{h}{2}}^{+\frac{h}{2}} \left(\sigma_{rr} d e_{rr} + \sigma_{\theta\theta}\delta\varepsilon_{\theta\theta} + \sigma_{rz}\beta_\gamma rz\right) dz dA$$
$$+ \int_A \left(K_w w_0 dw_0 + K_p\left(\frac{\partial w_0}{\partial r}\right)\left(\frac{\partial dw_0}{\partial r}\right)\right) dA$$
$$= \int_A \left(N_{rr}\left(\frac{\partial \delta u_0}{\partial r} + \frac{\partial w_0}{\partial r}\frac{\partial dw_0}{\partial r}\right) + M_{rr}\frac{\partial \delta\psi}{\partial r}\right.$$
$$\left. + N_{\theta\theta}\frac{\delta u_0}{r} + M_{\theta\theta}\frac{\delta\psi}{r} + N_{rz}\left(\frac{\partial \delta w_0}{\partial r} + \delta\psi\right)\right.$$
$$\left. + K_w w_0 \delta w_0 + K_p\left(\frac{\partial w_0}{\partial r}\right)\left(\frac{\partial \delta w_0}{\partial r}\right)\right) dA \qquad (19)$$

$$\delta K = \int_A \int_{-\frac{h}{2}}^{+\frac{h}{2}} \rho(z)\left(\dot{u}d\dot{u} + \dot{w}\delta\dot{w}\right) dz dA \qquad (20)$$
$$= \int_A \left(I_0\dot{u}_0\delta\dot{u}_0 + I_2\dot{\psi}\delta\dot{\psi} + I_0\dot{w}_0 d\dot{w}_0\right) dA$$
$$\delta V = \int_A q dw_0 dA \qquad (21)$$

By substituting Eqs. (19)-(21) into Hamilton's principle:

$$\int_0^T [\delta U - \delta K - \delta V]\, dt$$
$$= \int_0^T \left\{\int_{R_i}^{R_o} \left(N_{rr}\left(\frac{\partial \delta u_0}{\partial r} + \frac{\partial w_0}{\partial r}\frac{\partial \delta w_0}{\partial r}\right)\right.\right.$$
$$+ M_{rr}\frac{\partial \delta\psi}{\partial r} + N_{\theta\theta}\frac{\delta u_0}{r} + M_{\theta\theta}\frac{\delta\psi}{r}$$
$$+ N_{rz}\left(\frac{\partial \delta w_0}{\partial r} + \delta\psi\right) + K_w w_0 \delta w_0 \qquad (22)$$
$$+ K_p\left(\frac{\partial w_0}{\partial r}\right)\left(\frac{\partial \delta w_0}{\partial r}\right)$$
$$- \left(I_0\dot{u}_0\delta\dot{u}_0 + I_2\dot{\psi}\delta\dot{\psi} + I_0\dot{w}_0\delta\dot{w}_0\right)$$
$$\left.\left. - q dw_0\right) r dr\right\} dt = 0$$

By applying integration by parts and performing some mathematical simplification, Eqs. (22) can be rewritten in the following form:

$$\int_0^T \left\{\int_{R_i}^{R_o} \left(\left(\frac{\partial}{\partial r}(rN_{rr}) - N_{\theta\theta}\right)\delta u_0\right.\right.$$
$$+ \left(\frac{1}{r}\frac{\partial}{\partial r}\left(rN_{rr}\frac{\partial w_0}{\partial r}\right) + \frac{\partial N_{rz}}{\partial r} + \frac{N_{rz}}{r}\right.$$
$$\left. - K_w w_0 + K_p\left(\frac{\partial^2 w_0}{\partial r^2} + \frac{1}{r}\frac{\partial w_0}{\partial r}\right)\right)\delta w_0$$
$$+ \left(\frac{\partial M_{rr}}{\partial r} + \frac{M_{rr} - M_{\theta\theta}}{r} - N_{rz}\right)\delta\psi$$
$$\left. - \left(I_0\frac{\partial^2 u_0}{\partial t^2} + I_1\frac{\partial^2 \psi}{\partial t^2}\right)\delta u_0 - I_0\frac{\partial^2 w_0}{\partial t^2}{}_0 r dr\right\} dt = 0 \qquad (23)$$

By using the fundamental lemma of the calculus of variations in Eq. (23), the equation of motion for a relatively thick FG-CNT annular circular plate is obtained as follows:

$$\frac{1}{r}\left(\frac{\partial}{\partial r}(rN_{rr}) - N_{\theta\theta}\right) = I_0\frac{\partial^2 u_0}{\partial t^2} \qquad (24)$$

$$\frac{1}{r}\frac{\partial}{\partial r}\left(rN_{rr}\frac{\partial w_0}{\partial r}\right)+\frac{\partial N_{rz}}{\partial r}+\frac{N_{rz}}{r}-K_w w_0 + K_p\left(\frac{\partial^2 w_0}{\partial r^2}+\frac{1}{r}\frac{\partial w_0}{\partial r}\right)+q=I_0\frac{\partial^2 w_0}{\partial t^2} \quad (25)$$

$$\frac{\partial M_{rr}}{\partial r}+\frac{M_{rr}-M_{\theta\theta}}{r}-N_{rz}=I_2\frac{\partial^2\psi}{\partial t^2} \quad (26)$$

By substituting Eqs. (17) and (18) into Eqs. (24) to (26), nonlinear equations of motion are obtained in terms of displacements u_0, w_0 and ψ:

$$A_{11}\left(\frac{\partial^2 u_0}{\partial r^2}+\frac{\partial w_0}{\partial r}\frac{\partial^2 w_0}{\partial r^2}+\frac{1}{r}\frac{\partial u_0}{\partial r}+\frac{1}{2r}\left(\frac{\partial w_0}{\partial r}\right)^2\right) - A_{12}\frac{1}{2r}\left(\frac{\partial w_0}{\partial r}\right)^2-A_{22}\frac{u_0}{r^2}+B_{11}\left(\frac{\partial^2\psi}{\partial r^2}+\frac{1}{r}\frac{\psi}{\partial r}\right) - B_{22}\frac{\psi}{r^2} = I_0\frac{\partial^2 u_0}{\partial t^2} \quad (27)$$

$$\frac{1}{r}\frac{\partial}{\partial r}\left(r\left[A_{11}\left(\frac{\partial u_0}{\partial r}+\frac{1}{2}\left(\frac{\partial w_0}{\partial r}\right)^2\right)\frac{\partial w_0}{\partial r}+A_{12}\frac{u_0}{r}\frac{\partial w_0}{\partial r} + B_{11}\frac{\partial\psi}{\partial r}\frac{\partial w_0}{\partial r}+B_{12}\frac{\psi}{r}\frac{\partial w_0}{\partial r}\right]\right) + \frac{\partial}{\partial r}\left[A_{12}\left(\frac{\partial u_0}{\partial r}+\frac{1}{2}\left(\frac{\partial w_0}{\partial r}\right)^2\right)+A_{22}\frac{u_0}{r}+B_{12}\frac{\partial\psi}{\partial r} + B_{22}\frac{\psi}{r}\right] + \frac{1}{r}\left[A_{12}\left(\frac{\partial u_0}{\partial r}+\frac{1}{2}\left(\frac{\partial w_0}{\partial r}\right)^2\right) + A_{22}\frac{u_0}{r}+B_{12}\frac{\partial\psi}{\partial r}+B_{22}\frac{\psi}{r}\right]-K_w w_0 + K_p\left(\frac{\partial^2 w_0}{\partial r^2}+\frac{1}{r}\frac{\partial w_0}{\partial r}\right)+q=I_0\frac{\partial^2 w_0}{\partial t^2} \quad (28)$$

$$B_{11}\left(\frac{\partial^2 u_0}{\partial r^2}+\frac{\partial w_0}{\partial r}\frac{\partial^2 w_0}{\partial r^2}+\frac{1}{r}\frac{\partial u_0}{\partial r}+\frac{1}{2r}\left(\frac{\partial w_0}{\partial r}\right)^2\right) - B_{12}\frac{1}{2r}\left(\frac{\partial w_0}{\partial r}\right)^2-B_{22}\frac{u_0}{r^2}+D_{11}\left(\frac{\partial^2\psi}{\partial r^2}+\frac{1}{r}\frac{\partial\psi}{\partial r}\right) - D_{22}\frac{\psi}{r^2}-A_{55}\left(\psi+\frac{\partial w_0}{\partial r}\right)=I_2\frac{\partial^2\psi}{\partial t^2} \quad (29)$$

The boundary conditions of an annular circular plate with inner and outer elastic boundaries are as:

$$At \quad r=R_o \quad Q_{rr}=-K_{T1}w_0, \quad M_{rr}=-K_{R1}\psi, \quad u_0=0 \quad (30)$$

$$At \quad r=R_i \quad Q_{rr}=K_{T2}w_0 \quad M_{rr}=K_{R2}\psi, \quad u_0=0 \quad (31)$$

To normalize the equations, the following dimensionless parameters are defined:

$$\overline{w_0}=\frac{w_0}{h}, \quad \overline{u_0}=\frac{u_0}{h}, \quad x=\frac{r}{R_o}, \quad b=\frac{R_i}{R_o}, \quad \lambda=\frac{h}{R_o}$$
$$a_{ij}=\frac{A_{ij}h^2}{D_m}, \quad b_{ij}=\frac{B_{ij}h}{D_m}, \quad d_{ij}=\frac{D_{ij}}{D_m}, \quad \left(\overline{I}_0,\overline{I}_1,\overline{I}_1\right)=\left(\frac{I_0}{I_m}.\frac{I_1}{I_m h}.\frac{I_2}{I_m h^2}\right)$$
$$T_i=\frac{K_{T_i}R_o^3}{D_m}, \quad R_i=\frac{K_{R_i}R_o}{D_m}, \quad K_w=\frac{k_w R_o^4}{D_m}, \quad K_p=\frac{k_p R_o^2}{D_m}, \quad F=\frac{qR_o^4}{D_m h}$$
$$\tau=\frac{t}{R_o^2}\sqrt{\frac{D_m}{I_m}} \quad (32)$$

Finally, the dimensionless form of equations of motion are given as follows:

$$\frac{a_{11}}{\lambda^2}\left(\frac{\partial^2\overline{u_0}}{\partial x^2}+\lambda\frac{\partial\overline{w_0}}{\partial x}\frac{\partial^2\overline{w_0}}{\partial x^2}+\frac{1}{x}\frac{\partial\overline{u_0}}{\partial x}+\frac{\lambda}{2x}\left(\frac{\partial\overline{w_0}}{\partial x}\right)^2\right) - a_{12}\frac{1}{2x\lambda}\left(\frac{\partial\overline{w_0}}{\partial x}\right)^2-\frac{a_{22}}{\lambda^2}\frac{\overline{u_0}}{x^2}+\frac{b_{11}}{\lambda^2}\left(\frac{\partial^2\psi}{\partial x^2}+\frac{1}{x}\frac{\partial\psi}{\partial x}\right) - \frac{b_{22}}{\lambda^2}\frac{\psi}{x^2}=\overline{I}_0\frac{\partial^2\psi}{\partial t^2} \quad (33)$$

$$\frac{a_{55}}{\lambda^3}\left(\lambda\frac{\partial^2\overline{w_0}}{\partial x^2}+\frac{\lambda}{x}\frac{\partial\overline{w_0}}{\partial x}+\frac{\lambda}{x}+\frac{\partial\psi}{\partial x}\right) + \frac{a_{11}}{\lambda}\left(\frac{\partial\overline{u_0}}{\partial x}\frac{\partial^2\overline{w_0}}{\partial x^2}+\frac{\lambda}{2}\left(\frac{\partial\overline{w_0}}{\partial x}\right)^2\frac{\partial^2\overline{w_0}}{\partial x^2}+\frac{1}{x}\frac{\partial\overline{u_0}}{\partial x}\frac{\partial\overline{w_0}}{\partial x} + \frac{\lambda}{2x}\left(\frac{\partial\overline{w_0}}{\partial x}\right)^2\frac{\partial\overline{w_0}}{\partial x}+\frac{\partial^2\overline{u_0}}{\partial x^2}\frac{\partial\overline{w_0}}{\partial x}\right) \quad (34)$$

$$+\lambda\frac{\partial^2\overline{w_0}}{\partial x^2}\left(\frac{\partial\overline{w_0}}{\partial x}\right)^2+\frac{a_{12}}{\lambda}\left(\frac{\overline{u_0}}{x}\frac{\partial^2\overline{w_0}}{\partial x^2}+\left(\frac{1}{x}\frac{\partial\overline{u_0}}{\partial x}\right)\frac{\partial\overline{w_0}}{\partial x}\right) + \frac{b_{11}}{\lambda}\left(\frac{\partial\psi}{\partial x}\frac{\partial^2\overline{w_0}}{\partial x^2}+\frac{\partial^2\psi}{\partial x^2}\frac{\partial\overline{w_0}}{\partial x}+\frac{1}{x}\frac{\partial\psi}{\partial x}\frac{\partial\overline{w_0}}{\partial x}\right) + \frac{b_{12}}{\lambda}\left(\frac{\psi}{x}\frac{\partial^2\overline{w_0}}{\partial x^2}+\frac{1}{x}\frac{\partial\psi}{\partial x}\frac{\partial\overline{w_0}}{\partial x}\right)-K_w\overline{w_0} + K_p\left(\frac{\partial^2\overline{w_0}}{\partial x^2}+\frac{1}{x}\frac{\partial\overline{w_0}}{\partial x}\right)+F=\overline{I}_0\frac{\partial^2\overline{w_0}}{\partial t^2}$$

$$\frac{b_{11}}{\lambda^2}\left(\frac{\partial^2\overline{u_0}}{\partial x^2}+\lambda\frac{\partial\overline{w_0}}{\partial x}\frac{\partial^2\overline{w_0}}{\partial x^2}+\frac{1}{x}\frac{\partial\overline{u_0}}{\partial x}+\frac{\lambda}{2x}\left(\frac{\partial\overline{w_0}}{\partial x}\right)^2\right) - \frac{b_{12}}{2x\lambda}\left(\frac{\partial\overline{w_0}}{\partial x}\right)^2-\frac{b_{22}}{\lambda^2}\frac{\overline{u_0}}{x^2}+\frac{d_{11}}{\lambda^2}\left(\frac{\partial^2\psi}{\partial x^2}+\frac{1}{x}\frac{\partial\psi}{\partial x}\right) - \frac{d_{22}}{\lambda^2}\frac{\psi}{x^2}-\frac{a_{55}}{\lambda^4}\left(\psi+\lambda\frac{\partial\overline{w_0}}{\partial x}\right)=\overline{I}_2\frac{\partial^2\psi}{\partial t^2} \quad (35)$$

3. Generalized Differential Quadratic Method

Finding a closed-form solution for the current system equations is almost impossible. Hence, the GDQM is used to solve the differential equations of motion. By applying the GDQM and a fourth-order differential approximation, the partial differential equations of motion are transformed into a system of algebraic equations that can be solved as an eigenvalue problem. First, displacement components and their derivatives with respect to x are approximated as a summation of functions evaluated at all domain and boundary points [29]:

$$\left.\frac{\partial^m f(x)}{\partial x^m}\right|_{x=x_i} \approx \sum_{j=1}^{N} C_{ij}^{(m)} f(x_j), \qquad i=1,...,N \tag{36}$$

Where N denotes the number of discrete points, $f(x_j)$ represents the value of the function at the discrete point x_j, and $C_{ij}^{(m)}$ is the weight coefficients of the derivative of order m. To calculate the weighting coefficients $C_{ij}^{(m)}$, the adjoint Lagrange basis functions are used as test functions to obtain the implicit relation for the weighting coefficients [29]:

$$C_{ij}^{(1)} = \begin{cases} \frac{M^1(x_i)}{(x_i-x_j)M^1(x_j)} & i \neq j \\ -\sum_{j=1.\ j\neq i}^{N} C_{ij}^{(1)} & i=j \end{cases} \qquad (i,j=1,...,N) \tag{37}$$

whereas:

$$M^1(x_k) = \prod_{k=1,k\neq i}^{N} (x_k - x_i), \qquad i=1,...,N \tag{38}$$

In addition, the higher-order coefficient matrices are determined using the following relations [29]:

$$\begin{aligned} C_{ij}^{(2)} &= \sum_{k=1}^{N} C_{ik}^{(1)} C_{kj}^{(1)}, \qquad i,j=1,...,N \\ C_{ij}^{(3)} &= \sum_{k=1}^{N} C_{ik}^{(1)} C_{kj}^{(2)}, \qquad i,j=1,...,N \\ C_{ij}^{(4)} &= \sum_{k=1}^{N} C_{ik}^{(1)} C_{kj}^{3)}, \qquad i,j=1,...,N \end{aligned} \tag{39}$$

Then the axially symmetric circular plate is discretized into N points along the r-axis. Although using uniformly spaced points is the most straightforward approach, previous studies [29] have demonestrated that Chebyshev polynomial functions are suitable options for calculating the discrete points, which are defined as follows [29]:

$$r_i = \frac{R_o - R_i}{2}\left[1 - \cos(\frac{i-1}{N-1}p)\right] + R_i, \qquad i=1,...,N \tag{40}$$

The dimensionless form of the Eq. (40) is as follows [29]:

$$x_i = \frac{R_i}{R_o} + \frac{R_o - R_i}{2R_o}\left[1 - \cos\left(\frac{i-1}{N-1}p\right)\right], \ i=1,...,N \tag{41}$$

By means of GDQM, the system of nonlinear differential equations of motion, Eqs. (33) to (35), together with the boundary conditions, Eqs. (30) and (31), is transformed into a set of nonlinear algebraic type as follows:

$$[M]\left\{\ddot{X}\right\} = \left([K]_L + [K]_{NL}\right)\{X\} \tag{42}$$

Where $[M]$ is the mass matrix, $[K]_L$ and $[K]_{NL}$ are the linear and nonlinear elastic stiffness matrices, respectively.

After calculating the eigenvalues and eigenvectors by the GDQM, a polynomial function of degree n is attributed to the mode shape vector so that it is a suitable approximation for the mode shape function. As a result, the approximate analytical solution for calculating the nonlinear response of the system based on the proposed polynomial mode shape function is presented below:

$$\begin{aligned} \overline{u}(\overline{r},t) &= \overline{U(t)}\Phi(x) \\ \overline{\psi}(\overline{r},\tau) &= \overline{\psi(\tau)}\Phi(x) \\ \overline{w}(\overline{r},\tau) &= \overline{W(\tau)}\Phi(x) \\ \Phi(x) &= (a_n x^n + a_{n-1}x^{n-1} + a_{n-2}x^{n-2}\ldots \\ &\qquad + a_1 x + a_0)_{u,\psi,w} \end{aligned} \tag{43}$$

That the coefficients a_n are unknown and are extracted using the *polyfit* command in MATLAB, also, $\overline{W(\tau)}$ and $\overline{U(\tau)}$ and $\overline{\psi(\tau)}$ are the dimensionless time response along the z, r, and θ axes of the system, respectively. In order to convert the partial differential equations into the ordinary differential equations, the Galerkin method is applied. For this purpose, by substituting Eq. (43) into the Eqs. (33)-(35) and multiplying the equations by $\Phi(x)$ and then integrating over the domain of the plate, the nonlinear partial differential equations of the plate are changed to the ordinary differential equations as follows:

$$C_1\overline{U(t)} + C_2\overline{\Psi(\tau)} + C_3\overline{W(\tau)}^2 = C_5\overline{\ddot{\Psi}(t)} \tag{44}$$

$$\begin{aligned} &C_6\overline{W(\tau)} + C_7\overline{\Psi(\tau)} + C_8\overline{W(\tau)}^3 + C_9\overline{W(\tau)\Psi(\tau)} \\ &+ C_{10}\overline{U(t)W(\tau)} + C_{11}F = C_{12}\overline{\ddot{W}(\tau)} \end{aligned} \tag{45}$$

$$\begin{aligned} &C_{13}\overline{U(\tau)} + C_{14}\overline{W(\tau)} + C_{15}\ \overline{\Psi(\tau)} + C_{16}\overline{W(\tau)}^2 \\ &= C_{18}\overline{\ddot{\Psi}(t)} \end{aligned} \tag{46}$$

The Ci coefficients are given in Appendix A. In Eqs. (44)-(45) and (46), the terms $\overline{U(\tau)}$ and $\overline{\Psi(\tau)}$ are substitutingin terms of $\overline{W(\tau)}$. Then by inserting the terms $\overline{U(\tau)}$ and $\overline{\Psi(\tau)}$ in the Eq. (45), finally, the nonlinear differential equation of motion of the plate is:

$$\frac{d^2\overline{W}}{d\tau^2} + \mathrm{A}\ \overline{W} + \mathrm{B}\ \overline{W}^2 + \mathrm{C}\ \overline{W}^3 = \mathrm{D}F\sin(\Omega\tau) \quad (47)$$

where F and Ω are amplitude and frequency of the excitation, respectively, and A, B, C and D are given in Appendix B.

4. Multiple Time Scales Method

To investigate the forced vibrations of the system, the annular plate is assumed to be subjected to sinusoidal harmonic loading was assumed. Therefore, the equation of motion of the system is similar to Eq. (47).

Due to the non-linearity of Eq. (47), the method of multiple scales (MMS) is applied for the analytical solution. Accordingly, the excitation frequency near the first resonant frequency is investigated. Following the canonical approach of Nayfeh and Mook [32], the nonlinear and forcing terms are both scaled at order ϵ^2 to maintain a balanced perturbation expansion. This ensures that the nonlinear effects and resonant excitation contribute simultaneously to the modulation equations, enabling accurate analysis of the primary resonance behavior. Indeed, MMS is a perturbation technique that assumes the nonlinearity is moderate and the response can be expanded in terms of a small parameter. This makes it particularly well-suited for analyzing weakly nonlinear systems and capturing phenomena such as primary resonance with high accuracy. For cases involving strong nonlinearity, where the assumptions underlying MMS may no longer hold, alternative approaches such as numerical integration methods (e.g., direct time integration using Runge-Kutta schemes), harmonic balance methods with higher-order approximations, incremental harmonic balance, or non-perturbative analytical methods (e.g., shooting method, continuation methods) can indeed provide more accurate or globally valid solutions.

For primary resonance with the approximation of three terms, the nonlinear terms and the excitation force must all be of the same time order (ϵ^2). Accordingly, Eq. (47) is rewritten in the following form:

$$\frac{\partial^2\overline{W}}{\partial\tau^2} + \alpha\overline{W} + \epsilon^2\hat{\beta}\overline{W}^2 + \epsilon^2\hat{\gamma}\overline{W}^3 = \epsilon^2\hat{F}\sin(\Omega t) \quad (48)$$

where the coefficients of $\hat{\beta}$, $\hat{\gamma}$ and F^ are as follows:

$$\alpha = A, \qquad \hat{\beta} = \frac{\beta}{\epsilon^2}, \qquad \hat{\gamma} = \frac{\mathrm{C}}{\epsilon^2}, \qquad \hat{F} = \mathrm{D}\ F/\epsilon^2 \quad (49)$$

The excitation frequency is assumed to be near the primary resonance (fundamental natural frequency) of the system, using the term σ as the detuning parameter, as follows [30]:

$$\Omega = \omega + \epsilon^2\sigma \quad (50)$$

The independent time variables T_n and the response of the system W are expanded as follows [30]:

$$T_n = \epsilon^n t \quad for \quad n = 0,\ 1,\ 2,\ \ldots \quad (51)$$

$$W = W_0(T_0, T_1, T_2) + \epsilon W_1(T_0, T_1, T_2) + \epsilon^2 W_2(T_0, T_1, T_2) + O(\epsilon^3) \quad (52)$$

A series of partial derivatives concerning T_n are used instead of the derivatives in terms of t as follows [30]:

$$\begin{aligned} \frac{d}{dt} &= D_0 + \epsilon D_1 + \epsilon^2 D_2. \\ \frac{d^2}{dt^2} &= D_0^2 + 2\epsilon D_0 D_1 + \epsilon^2\left(D_1^2 + 2D_0 D_2\right) \\ D_n &= \frac{\partial}{\partial T_n} \end{aligned} \quad (53)$$

By substituting Eq. (51) to (53) in Eq. (48) and separating the coefficients of ϵ, the following set of equations are obtained:

$$D_0^2 W_0 + \omega^2 W_0 = 0 \quad (54)$$

$$D_0^2 W_1 + \omega^2 W_1 = -2D_0 D_1 W_0 - \hat{\beta} W_0^2 \quad (55)$$

$$D_0^2 W_2 + \omega^2 W_2 = -2D_0 D_1 W_1 - 2D_0 D_2 W_0 - D_1^2 W_0 - 2\hat{\beta} W_0 W_1 - \hat{\gamma} W_0^3 \quad (56)$$

The general solution of Eq. (54) is as follows:

$$W_0 = A(T_1, T_2)\, exp(i\omega T_0) + cc \quad (57)$$

where A is the amplitude of the system vibration in terms of T_1 and T_2, and the term cc is the complex conjugate of the response.

Substituting Eq. (57) into Eq. (55):

$$D_0^2 W_1 + \omega^2 W_1 = -2i\omega\left(D_1 A\right)\exp(i_0) - \hat{\beta}\left(A^2 exp(2i_0) + A\overline{A}\right) + cc \quad (58)$$

where $\overline{A}$ is the complex conjugate of A. By removing the secular terms from Eq. (58):

$$2i\omega D_1 A = 0 \quad (59)$$

By solving Eq. (59), A is obtained as follows:

$$A = A(T_2) \quad (60)$$

Solution of Eq. (58) leads to the following answer:

$$W_1 = \frac{\hat{\beta}}{\omega^2}\left(\frac{1}{3}A^2\exp(2i\omega T_0) - A\ \overline{A}\right) + cc \quad (61)$$

Table 1
Roperties of the matrix and the reinforcing part of the plate [8].

Base material (PMMA)			Reinforcement (CNTs)				
$E^m(Gpa)$	$\rho^m\left(\frac{kg}{m^3}\right)$	v^m	$E_{11}^{cnt}(Tpa)$	$E_{22}^{cnt}(Tpa)$	$G_{12}^{cnt}(Tpa)$	$\rho^{cnt}\left(\frac{kg}{m^3}\right)$	v_{12}^{CNT}
2.5	1150	0.34	5.6466	7.0800	1.9445	1400	0.175

Substituting Eq. (57) and (61) into Eq. (56):

$$D_0^2W_2+\omega^2W_2=-\left(2i\omega\left(D_2A\right)+\left(3\hat{\gamma}-\frac{10\hat{\beta}^2}{3\omega^2}\right)A^2\overline{A}\right.$$
$$-\frac{1}{2}\hat{F}\exp\left(i\sigma T_2\right)\exp\left(i\omega T_0\ \right)$$
$$+\text{Nonsecular terms}+cc \tag{62}$$

The secular terms in Eq. (62) must be omitted to have a harmonic response, hence:

$$2i\omega\left(D_2A\right)+\left(3\hat{\gamma}-\frac{10\hat{\beta}^2}{3\omega^2}\right)A^2\overline{A}-\frac{1}{2}\hat{F}\exp\left(i\sigma T_2\right)=0 \tag{63}$$

Considering $A=\frac{1}{2}a\left(T_2\right)\exp\left(\phi\left(T_2\right)i\right)$ and substituting in Eq. (63), this equation could be rewritten into two non-autonomous system of equations, after separating imaginary and real terms as follows:

$$a'=\frac{\hat{F}}{2\omega}\sin(\sigma T_2-\phi)$$
$$a(\sigma T_2-\phi)'=a\sigma-\left(\frac{9\gamma\omega^2-10\beta^2}{24\omega^2}\right)a^3 \tag{64}$$
$$+\frac{\hat{F}}{2\omega}\cos(\sigma T_2-\phi)$$

This non-autonomous system of equations must be transformed into autonomous equations. In order to have a steady-state response, $a'=\phi'=0$ is assumed. Accordingly, Eqs. (64) and (65) are transformed into the following form:

$$\left(\left(\sigma-\left(\frac{9\gamma\omega^2-10\beta^2}{24\omega^2}\right)a^2\right)^2\right)a^2=\frac{F^2}{4\omega^2} \tag{65}$$

5. Results and Discussion

5.1. Validation of Results

Following the modeling, formulation of the governing equations of the problem, and analytical solution of the system, the validation and the results are presented.

To compare the nonlinear frequencies of the circular plate reinforced by CNTs, only one relevant reference was found [8], although in this reference the circular plate is considered as a sandwich structure in which the top and bottom face sheets are CNT-reinforced circular plates with a thickness of h_f, and the middle plate that forms the core of the sandwich structure is made of a homogeneous circular plate of titanium alloy with a thickness of h_c. Also, the whole plate is placed on Winkler and Pasternak elastic substrates. The total thickness of the sandwich plate is $h=h_c+2h_f$. The mechanical properties of CNTs are listed in Table 1. Also, the efficiency parameters related to CNTs are presented in Table 2. In addition, the properties of titanium alloy are shown in Table 3. Table 4 compares the nonlinear to linear natural frequency ratio ($\omega_{NL}\omega_L$) and also the linear frequency (in Hz) of the circular sandwich plate reinforced with CNTs with the uniform distribution pattern of CNTs with girder–girder boundary conditions, as reported in [8]. In comparison, the plate specifications are considered as R_i=2.5, R_o=5, V_{CNT}=0.17, h_c/h_f=4, $K_w=25\times12/h^2$, and $K_p=2.5\times12/h^2$. These results are very accurate, as can be seen from the table.

In this section, the system's dynamic response is validated in a specific mode. In order to validate the results of the nonlinear forced vibrations of the system, in this part, the dynamic response of the annular plate under high-amplitude harmonic loading is calculated and compared using three methods, the analytical method of multiple time scales, the Adams-Bashforth numerical method, and Abaqus software. In this part, a homogeneous annular plate with the clamped-clamped boundary conditions and the mechanical properties of $E=380$GPa, $\rho=3800$Kg/m^3, and $v=0.3$ are modeled in Abaqus software. The outer radius, inner radius, and plate thickness are taken as 1m, 0.5m and 0.04m, respectively.

Table 2
Performance parameters of CNTs [8].

V_{cnt}^*	η_1	η_2	η_3
0.12	0.137	1.022	0.715
0.17	0.142	1.626	1.138
0.28	0.141	1.585	1.109

Table 3
Mechanical properties of titanium alloy [8].

	Density (Kg/m^3)	Elastic Modulus (GPa)	Poisson's coefficient
Mechanical properties	4429	105.6982	0.29

Table 4
Validation of nonlinear to linear natural frequency ratio ($\omega_{NL}\omega_L$) as well as linear frequency ω_L (in Hz) of the circular sandwich plate reinforced with CNTs with a uniform UD distribution pattern.

			$\omega_{NL}/\omega L$		
			W_{max}/h		
	h/R_o	ω_L (Hz)	0.4	0.7	1
Current study	0.04	202.868	1.05269	1.15288	1.29123
[8]		202.867	1.05272	1.15297	1.29140
Current study	0.06	273.229	1.06030	1.17380	1.32879
[8]		273.228	1.06012	1.17338	1.32817
Current study	0.08	328.786	1.06862	1.19662	1.36899
[8]		328.786	1.06848	1.19611	1.36861
Current study	0.10	370.935	1.07995	1.22681	1.42235
[8]		370.934	1.07948	1.22557	1.42019

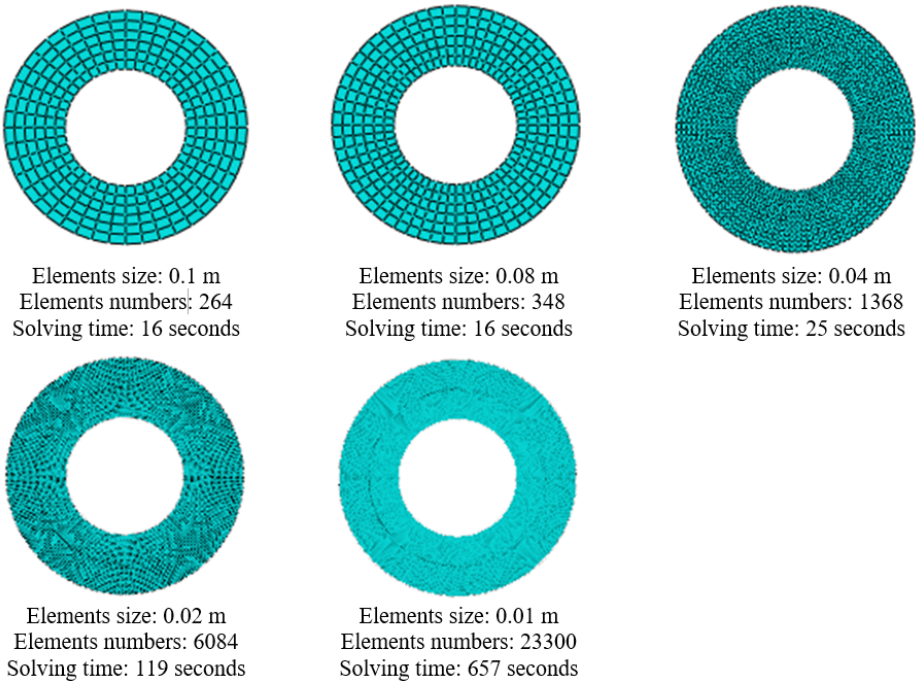

Fig. 3. Meshed plate in Abaqus software with different valuesof size and number of elements.

A sinusoidal harmonic load with an amplitude of 400 MPa and an excitation frequency of 2500rad/s is applied to the plate. In the Adams-Bashforth method, the total response time is set to 0.01sec with a time step of 7×10^{-10} seconds. The time step was validated through a convergence study, where the time step was progressively reduced until the changes in the computed responses (displacement amplitudes and frequency content) became negligible. This approach confirmed that this value provides a stable and accurate solution without excessive computational cost. It should be noted that the dynamic response of the plate is calculated at the position of $r = 0.75$m.

Before presenting the Abaqus results, a convergence study was conducted to examine the effect of element size. For this purpose, S4R-type elements were used in Abaqus and the sheet was meshed using the structured method, which provides the highest accuracy among available meshing methods. Also, the Dynamic/Explicit solver was employed with NLGeom: ON mode enabled to account for geometric nonlinearity. Fig. 3 shows the meshed plate in Abaqus with different element sizes, the total number of elements, as well as the corresponding solution times. Eventually, Fig. 4 compares the dynamic response of the plate under harmonic loading for different element size values. As it is clear from this figure, by reducing the size of the elements from 0.1 to 0.01m, the nonlinear dynamic response converges to a specific curve. However, an element size of 0.02m was selected for further simulations. Because in this case, the accuracy of the answer is high and the duration of the computer solution is 119sec, while the duration of the computer solution for the element size of 0.01m is 657sec, which is very time-consuming.

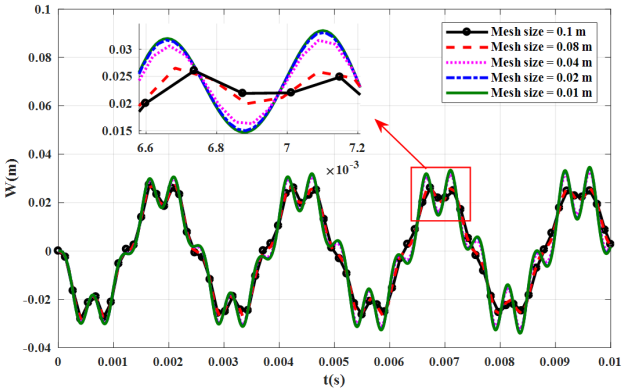

Fig. 4. Investigating the convergence of nonlinear dynamic response of sheet under harmonic loading in Abaqus.

Fig. 5. compares the linear dynamic response of the plate under harmonic loading with two numerical methods and Abaqus. As shown, the results exhibit excellent agreement. Fig. 6. compares the nonlinear dynamic response of the plate under harmonic loading with two numerical methods and Abaqus. As can be seen from this figure, the results are in very good congruence.

To solve the nonlinear dynamic equations resulting from the method of multiple scales, the explicit Adams-Bashforth numerical method is employed. This multi-step integration scheme uses derivative information from previous time steps to advance the solution efficiently and accurately, making it well-suited for capturing the transient nonlinear response near primary resonance.

Since spring elements cannot be modeled using the Dynamic/Explicit solver in Abaqus, and no reliable reference is available for comparing the current system, the nonlinear governing equations are solved twice: once using the Adams-Bashforth method with a time step of 6×10^{-10} seconds, and once using the analytical method of multiple time scales, and the answers are then compared with each other. Fig. 7. compares the nonlinear dynamic response of the CNT-reinforced plate with elastic boundaries subjected to sinusoidal harmonic loading with a dimensionless amplitude of 1500000 and an excitation frequency of 7000 using both numerical methods, Adams-Bashforth and the analytical method of multiple time scales for the uniform distribution pattern of nanotubes. The CNT volume fraction is taken as $VCNT = 0.28$. In this comparison, the ratio of inner-to-outer radius and the ratio of thickness-to-outer radius of the plate are 0.5 and 0.04, respectively, and also the mechanical properties of the plate are taken from Tables 1 and 2. Boundary elastic coefficients are set as $T1 = T2 = R1 = R2 = 5000$, and the elastic foundation coefficients are as $Kw = Kp = 100$. It should be noted that the dynamic response of the sheet is calculated at the position of r=0.75m. As shown in this figure, the numerical and analytical results are in well congruence.

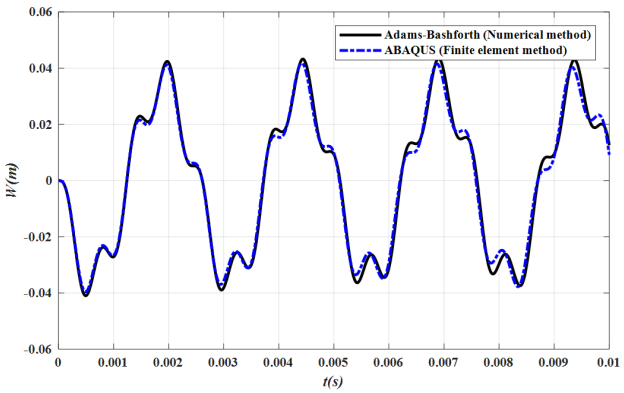

Fig. 5. Comparison of the linear dynamic response of plate under harmonic loading with the numerical method and Abaqus.

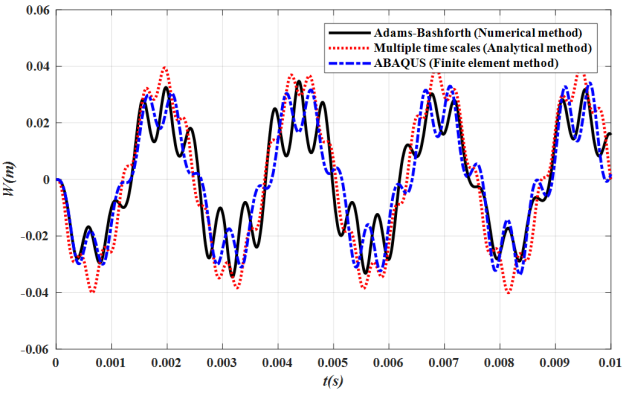

Fig. 6. Comparison of the nonlinear dynamic response of plate under harmonic loading with two numerical methods and Abaqus.

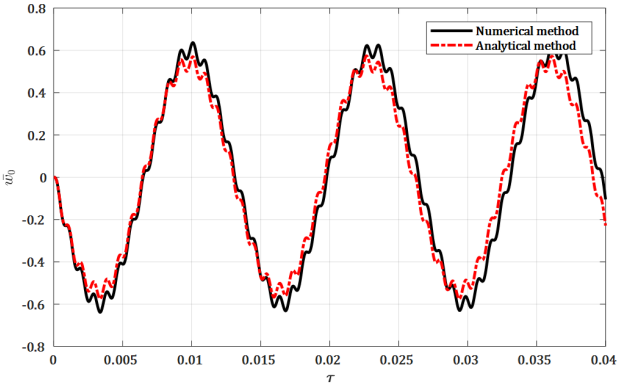

Fig. 7. Comparing the nonlinear forced response of CNTs reinforced plate with two analytical and numerical methods.

5.2. Effect of CNT Distribution

Fig. 8 illustrates the influence of the volume fraction of CNTs on nonlinear dynamic response and phase plane

of the reinforced plate by a uniform distribution pattern of CNTs along with elastic boundaries under extensive sinusoidal harmonic loading with a dimensionless amplitude of 1500000 and excitation frequency of 7000. In this investigation, the specifications of the annular plate are considered as $Kw = Kp = 100$, $h/Ro = 0.04$, $Ri/Ro = 0.5$, with elastic boundary coefficients $T1 = T2 = R1 = R2 = 5000$. Fig. 8a. Shows that the addition of CNTs to the plate causes the frequency of the time response to be increased, because by increasing the volume fraction of nanoparticles, the overall stiffness of the structure increases. In addition, it is clear from this graph that the vibration amplitude of the plate with a volume fraction of 0.12 of nanoparticles is 44% lower than the vibration amplitude of the plate without nanoparticles. By increasing the volume fraction of nanoparticles from 0.12 to 0.17, the vibration amplitude decreases by 10%, and also by increasing the volume fraction of nanoparticles from 0.12 to 0.28, the vibration amplitude decreases by 21%. According to this figure, it is found out that maximum amplitude occurs at t=0.007s. Furthermore, from the phase plane diagram in Fig. 8b. which shows a periodic movement for all three modes, similar results regarding the vibration amplitude are extracted.

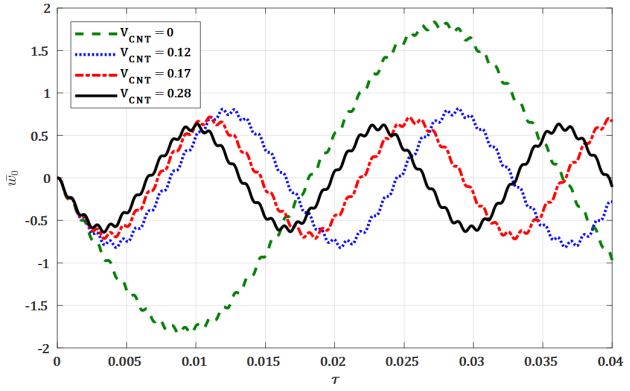

(a)

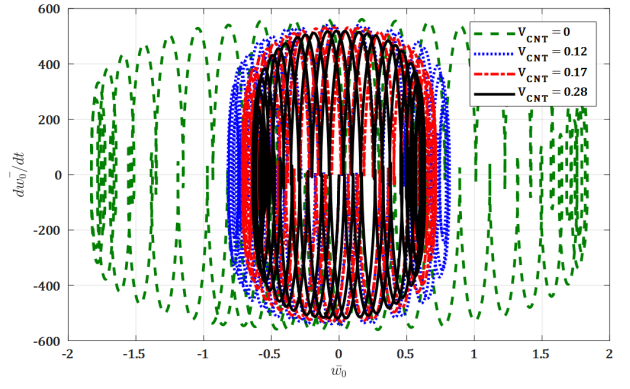

(b)

Fig. 8. The effect of volume fraction of nanoparticles on the nonlinear dynamic behavior of the plate under sinusoidal harmonic load a) time response b) phase plane.

It is also clear from this figure that by increasing the volume fraction of nanoparticles from 0.12 to 0.28, the rate of fluctuations is decreased by about 2%. The figure also shows that increasing the volume fraction of nanoparticles has a slight effect on the frequency of oscillations; however, it ultimately reduces the frequency of the structure's vibration.

The influence of the CNT distribution pattern on nonlinear dynamic response and phase plane of a plate reinforced with CNTs under elastic boundaries and extensive sinusoidal harmonic loading with a dimensionless amplitude of 1500000 and excitation frequency of 7000 is shown in Fig. 9. In this study, the specifications of the annular plate are considered as $Kw = Kp = 100$, $h/Ro = 0.04$, $Ri/Ro = 0.5$, and $VCNT = 0.28$ with elastic boundary coefficients $T1 = T2 = R1 = R2 = 5000$. The results of Fig. 9a. show that the dynamic response frequency of the plate with FGV and FGA distribution patterns is higher than the rest. However, the plate vibration amplitude with FGV and FGA distribution patterns is up to 70% lower than the others. The behavior of the vibration amplitude of the samples is also clear in the phase plane diagram of Fig. 9b. It is also clear from this graph that the speed of plate fluctuations with FGV and FGA distribution patterns is 28% lower than that of the other configurations.

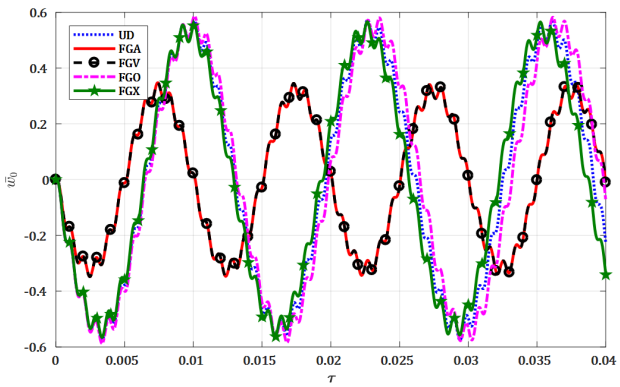

(a)

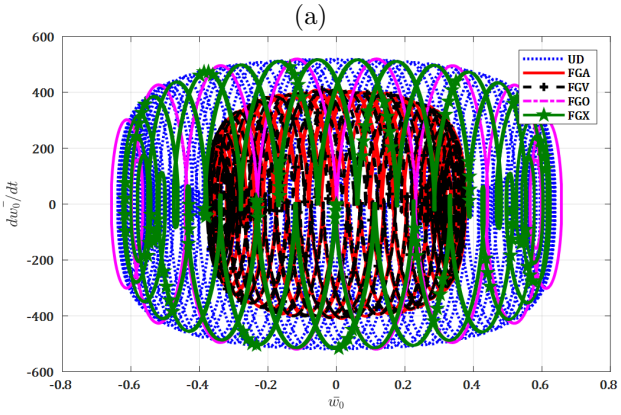

(b)

Fig. 9. The effect of nanoparticle distribution pattern on the nonlinear dynamic behavior of the plate under sinusoidal harmonic load a) time response b) phase plane.

5.3. Effect of Foundation Type

Fig. 10 shows the influence of the Winkler coefficients on the nonlinear dynamic response as well as the phase plane of the plate reinforced with CNTs with a uniform distribution pattern of elastic boundaries under extensive sinusoidal harmonic loading with a dimensionless amplitude of 1500000 and the excitation frequency of 7000. In this investigation, the specifications of the annular plate are considered as $VCNT = 0.28$, $Kp = 10$, $h/Ro = 0.04$, $Ri/Ro = 0.5$, with elastic boundary coefficients $T1 = T2 = R1 = R2 = 5000$. The results of these figures show that as the Winkler coefficient increases, the response frequency of the system is also increased because it increases the overall stiffness of the system, but it does not have a great effect on the amplitude and frequency.

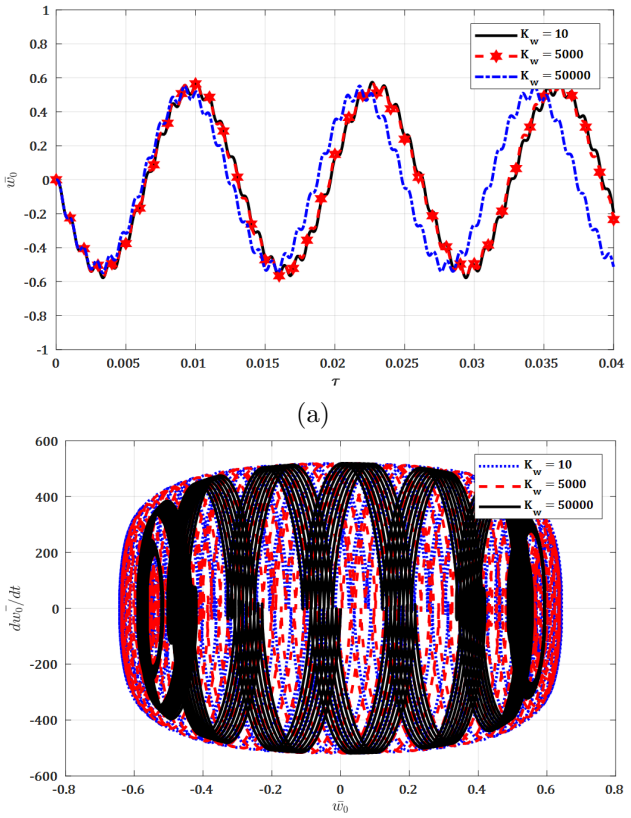

Fig. 10. The effect of the Winkler coefficient on the nonlinear dynamic behavior of the plate under sinusoidal harmonic load a) Time response b) Phase plane.

Fig. 11 exhibits the influence of Pasternak coefficients on the nonlinear dynamic response and phase plane of the plate reinforced with CNTs with uniform distribution pattern of elastic boundaries under extensive sinusoidal harmonic loading with a dimensionless amplitude of 1500000 and the excitation frequency of 7000. In this investigation, the specifications of the annular plate are considered as $VCNT = 0.28$, $Kw = 10$, $h/Ro = 0.04$, $Ri/Ro = 0.5$, with boundary coefficients $T1 = T2 = R1 = R2 = 5000$. The results show that with the increase of the Pasternak coefficient, the response frequency of the system increases because the overall stiffness of the structure increases. Also, the phase plane diagram in Fig 11b. shows that by increasing the Pasternak coefficient from 10 to 5000, the amplitude of vibrations decreases by 21% and also by increasing the Pasternak coefficient from 10 to 50000, the amplitude of vibrations decreases by 65%. But the fluctuation speed range remained unchanged despite the changes in the Pasternak coefficient.

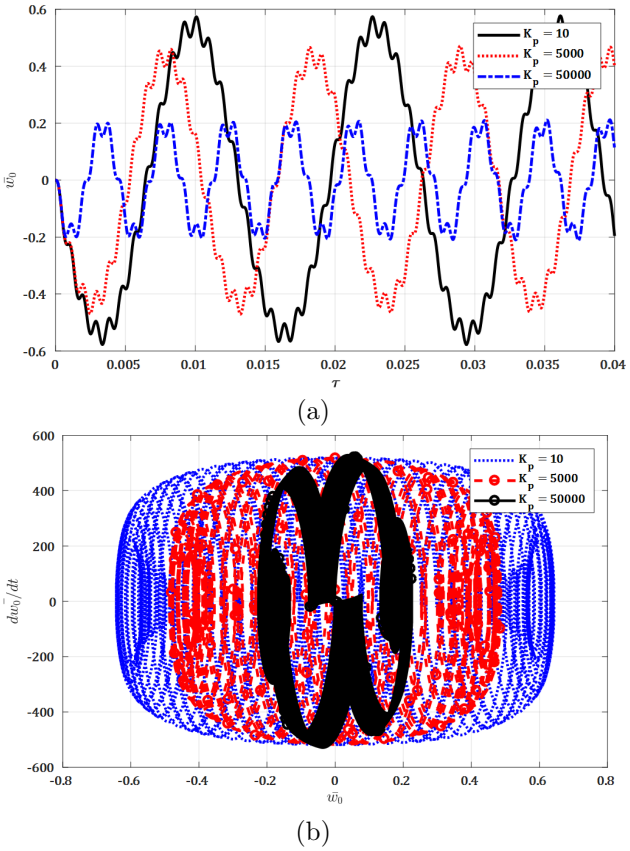

Fig. 11. The effect of the Pasternak coefficient on the nonlinear dynamic behavior of the plate under sinusoidal harmonic load a) Time response b) Phase plane.

6. Conclusion

In this study, the nonlinear forced vibrations of composite annular plates reinforced with CNTs subjected to elastic boundary conditions under harmonic load and half-sine pulse were analyzed analytically based on the FSDT. To achieve this, the equations of motion were derived based on the FSDT and Von Kármán's displacement–strain relations and were solved using GDQM and multiple time scales, and Adams-Bashforth. The most important results of this research are as follows:

1. As the volume fraction of CNTs increases, the frequency of the nonlinear dynamic response of the plate under harmonic and pulse loading is increased, and the amplitude of vibrations is decreased to some extent.

2. The influence of the distribution pattern of the nanoparticle on the nonlinear forced response of the plate under harmonic and pulse loading showed that the FGA and FGV have the lowest vibration amplitude among all cases, respectively.

3. The effect of the Winkler's bed on the non-linear forced response of the plate under harmonic and pulse load showed that increasing the stiffness coefficient of the Winkler bed causes the response frequency to be increased.

4. The influence of the Pasternak foundation on the non-linear forced response of the plate under harmonic and pulse loading showed that increasing the stiffness coefficient of Pasternak foundation leads to an increase in the frequency and a decrease in the vibration response amplitude.

Appendix A.

$$C_1 = \int_b^1 \left(\frac{a_{11}}{\lambda^2}\left(H_u^{''} + H_u'/x\right) - \frac{a_{22}}{\lambda^2 x^2}H_u\right) H_u x \; dx$$

$$C_2 = \int_b^1 \left(\frac{b_{11}}{\lambda^2}\left(H_\Psi^{''} + H_\Psi'/x\right) - \frac{b_{22}}{\lambda^2 x^2}H_\Psi\right) H_u x \; dx$$

$$C_3 = \int_b^1 \left(\frac{a_{11}}{\lambda}\left(H_w' H_w^{''} + {H_w'}^2/2x\right) - \frac{a_{12}}{2\lambda x}{H_w'}^2\right) H_u x dx$$

$$C_4 = \int_b^1 \overline{I_0} H_u^2 x \; dx$$

$$C_5 = \int_b^1 \overline{I_1} H_\Psi H_u x \; dx$$

$$C_6 = \int_b^1 \left(\frac{a_{55}}{\lambda^2}\left(H_w^{''} + H_w'/x\right) - \frac{a_{22}}{\lambda^2 x^2}H_u - K_w H_w + K_p(H_w^{''} + H_w'/x)\right) H_w x \; dx$$

$$C_7 = \int_b^1 \frac{a_{55}}{\lambda^3}\left(H_\Psi' + H_\Psi/x\right) H_w x \; dx$$

$$C_8 = \int_b^1 a_{11}\left(\frac{3}{2}H_w^{''}{H_w'}^2 + {H_w'}^3/2x\right) H_w x \; dx$$

$$C_9 = \int_b^1 \left(\frac{b_{11}}{\lambda}\left(H_w^{''}H_\Psi' + H_w' H_\Psi^{''} + H_w' H_\Psi'/x\right) + \frac{b_{12}}{\lambda}\left(H_w^{''}H_\Psi + H_w' H_\Psi'/x\right)\right) H_w x \; dx$$

$$C_{10} = \int_b^1 \left(\frac{a_{11}}{\lambda}\left(H_w^{''}H_u' + H_u' H_w'/x + H_u^{''}H_w'\right) + \frac{a_{12}}{\lambda}\left(H_w^{''}H_u + H_w' H_u'/x\right)\right) H_w x \; dx$$

$$C_{11} = \int_b^1 H_w \; x \; dx$$

$$C_{12} = \int_b^1 \overline{I_0} \; H_w^2 \; x \; dx$$

$$C_{13} = \int_b^1 \left(\frac{b_{11}}{\lambda^2}\left(H_u^{''} + H_u'/x\right) - \frac{b_{22}}{\lambda^2 x^2}H_u\right) H_\Psi \; x \; dx$$

$$C_{14} = -\int_b^1 \left(\frac{a_{55}}{\lambda^3}H_w'\right) H_\Psi \; x \; dx$$

$$C_{15} = \int_b^1 \left(\frac{d_{11}}{\lambda^2}\left(H_\Psi^{''} + H_\Psi'/x\right) - \frac{H_\Psi}{\lambda^2}\left(d_{22}/x^2 + a_{55}/L^2\right)\right) H_\Psi \; x \; dx$$

$$C_{16} = \int_b^1 \left(\frac{b_{11}}{\lambda}\left(H_w^{''}H_w' + {H_w'}^2/2x\right) - \frac{b_{12}}{2\mathrm{x}\lambda}{H_w'}^2\right) H_\Psi \; x \; dx$$

$$C_{17} = \int_b^1 \overline{I_1} H_\Psi \; H_u \; x \; dx$$

$$C_{18} = \int_b^1 \overline{I_2} H_\Psi^2 x dx$$

Appendix B.

$$\mathrm{A} = -\frac{C_6}{C_{12}} - \frac{C_1 C_7 C_{14}}{C_{12}(C_2 C_{13} - C_1 C_{15})}$$

$$\mathrm{B} = \frac{C_3 C_7 C_{13}}{C_{12}(C_2 C_{13} - C_1 C_{15})} - \frac{C_1 C_7 C_{16}}{C_{12}(C_2 C_{13} - C_1 C_{15})} - \frac{C_1 C_9 C_{14}}{C_{12}(C_2 C_{13} - C_1 C_{15})} + \frac{C_2 C_{10} C_{14}}{C_{12}(C_2 C_{13} - C_1 C_{15})}$$

$$\mathrm{C} = -\frac{C_8}{C_{12}} - \frac{C_1 C_9 C_{16}}{C_{12}(C_2 C_{13} - C_1 C_{15})} + \frac{C_2 C_{10} C_{16}}{C_{12}(C_2 C_{13} - C_1 C_{15})} + \frac{C_3 C_9 C_{13}}{C_{12}(C_2 C_{13} - C_1 C_{15})} - \frac{C_3 C_{10} C_{15}}{C_{12}(C_2 C_{13} - C_1 C_{15})}$$

$$\mathrm{D} = -\frac{C_{11}}{C_{12}}$$

References

[1] V. Mahesh, D. Harursampath, Nonlinear vibration of functionally graded magneto-electro-elastic higher order plates reinforced by CNTs using FEM, Eng. Comput., 38(2) (2022) 1029-1051.

[2] V. M. Kuriakose, P. R. Sai, M. S. Kumar, V. M. Sreehari, Influence of CNT fillers in the vibration characteristics of natural fiber reinforced composite plates, Compos. Struct., 282 (2022) 115012.

[3] R. Kumar, A. Kumar, Free vibration response of cnt-reinforced multiscale functionally graded plates using the modified shear deformation theory, Adv. Mater. Process. Technol, 8(4) (2022) 4257-4279.

[4] L. K. Sharma, N. Grover, G. Bhardwaj, Buckling and free vibration analysis of temperature-dependent functionally graded CNT-reinforced plates, J. Vib. Eng. Technol., 11(1) (2023) 175-192.

[5] Y. Zhang, W. Liu, Nonlinear vibration response of a functionally graded carbon nanotube-reinforced composite conical shell using a stress function method, Acta Mech., 233(8) (2022) 3157-3174.

[6] H. Afshari, H. Amirabadi, Vibration characteristics of rotating truncated conical shells reinforced with agglomerated carbon nanotubes, J. Vib. Control., 28(15-16) (2022) 1894-1914.

[7] S. Sun, C. Guo, W. Feng, D. Cao, Nonlinear vibration analysis of CNT-reinforced functionally graded composite cylindrical shells resting on elastic foundations, J. Non-Linear Mech., 143 (2022) 104037.

[8] R. Ansari, J. Torabi, E. Hasrati, Axisymmetric nonlinear vibration analysis of sandwich annular plates with FG-CNTRC face sheets based on the higher-order shear deformation plate theory, Aerosp. Sci. Technol., 77 (2018) 306-319.

[9] B. Uspensky, K. Avramov, N. Sakhno, O. Nikonov, Dynamic instability of functionally graded carbon nanotubes-reinforced composite joined conical-cylindrical shell, Int. J. Struct. Stab. Dyn., 22(07) (2022) 2250039.

[10] M. Avey, N. Fantuzzi, A. H. Sofiyev, N. Kuruoglu, Influences of elastic foundations on the nonlinear free vibration of composite shells containing carbon nanotubes within shear deformation theory, Compos. Struct., 286 (2022) 115288.

[11] S. Hashemi, P. K. Shahri, S. Beigzadeh, F. Zamani, M. G. Eratbeni, M. Mahdavi, M. R. R. Abadi, Nonlinear free vibration analysis of In-plane Bi-directional functionally graded plate with porosities resting on elastic foundations, Int. J. Appl. Mech., 14(01) (2022) 2150131.

[12] S. Hashemi, A. A. Jafari, An analytical solution for nonlinear vibrations analysis of functionally graded plate using modified Lindstedt-Poincare method, Int. J. Appl. Mech. 12(01) (2020) 2050003.

[13] B. Qin, R. Zhong, T. Wang, Q. Wang, Y. Xu, Z. Hu, A unified Fourier series solution for vibration analysis of FG-CNTRC cylindrical, conical shells and annular plates with arbitrary boundary conditions, Compos. Struct., 232 (2020) 111549.

[14] R. Ansari, J. Torabi, M. Faghih Shojaei, Free vibration analysis of embedded functionally graded carbon nanotube-reinforced composite conical/cylindrical shells and annular plates using a numerical approach, J. Vib. Control., 24(6) (2018) 1123-1144.

[15] L. W. Zhang, Z. X. Lei, K. M. Liew, Computation of vibration solution for functionally graded carbon nanotube-reinforced composite thick plates resting on elastic foundations using the element-free IMLS-Ritz method, Appl Math Comput., 256 (2015) 488-504.

[16] G. Stephan, S. Marco, G,G, Alberto, D. Pedro, R. Matas, F. Jose, Inverse Nonlinear Elastostatic Analysis of Heterogeneous Pre-Stressed Arterial Cross-Sections with Elastic Bed Supports: An Unfitted Approach, (2025). Available at SSRN: https://ssrn.com/abstract=5170675 or http://dx.doi.org/10.2139/ssrn.5170675.

[17] N. Togun, S. M. Bağdatlı, Nonlinear vibration of a nanobeam on a Pasternak elastic foundation based on non-local Euler-Bernoulli beam theory, Math. comput. appl., 21(1) (2016) 3.

[18] Q. Li, D. Wu, X. Chen, L. Liu, Y. Yu, W. Gao, Nonlinear vibration and dynamic buckling analyses of sandwich functionally graded porous plate with graphene platelet reinforcement resting on Winkler-Pasternak elastic foundation, Int. J. Mech. Sci., 148 (2018) 596-610.

[19] S. Parida, S. C. Mohanty, Nonlinear free vibration analysis of functionally graded plate resting on elastic foundation in thermal environment using higher order shear deformation theory, Sci. Iran., 26(2) (2019) 815-833.

[20] S. Shahsavari, S. Boutorabi, Nonlinear nonlocal damped free and forced vibrations of piezoelectric SWCNTs under longitudinal magnetic field due to surface effects using a two steps perturbation method, MOJ App Bio Biomech., 7(1) (2023) 88-99.

[21] M. G. Sobamowo, J. O. Akanmu, O. A. Adeleye, A. A. Yinusa, Nonlinear vibrations of single-and double-walled carbon nanotubes resting on two-parameter foundation in a magneto-thermal environment, SN Applied Sciences, 1(10) (2019) 1173.

[22] M. Azhdarzadeh, R. Jahangiri, A. Allahverdizadeh, B. Dadashzadeh, R. Nabati, Investigation of nonlinear thermo-elastic behavior of fluid conveying piezoelectric microtube reinforced by functionally distributed carbon nanotubes on viscoelastic-hetenyi foundation, Eur. J. Comput. Mech., 31(1) (2022) 65-100.

[23] H. Jafary, M. Taghizadeh, Nonlinear dynamics response of porous functionally graded annular plates using modified higher order shear deformation theory, SN Appl. Sci., 5(12) (2023) 368.

[24] T. Ma, J.X. Song, S. Fenh, Nonlinear Dynamics Modeling and Subharmonic Resonances Analysis of a Laminated Composite Plate, Shock and vibration, (2020) 1-16.

[25] A. Allahverdizadeh, M. H. Naei, M. N. Bahrami, Nonlinear free and forced vibration analysis of thin circular functionally graded plates, J. Sound Vib., 310(4-5) (2008) 966-984.

[26] M. Shadmani, A. Afsari, R. Jahedi, M. J. Kazemzadeh-Parsi, Nonlinear dynamic response of truncated conical shells reinforced with carbon nanotubes with functional graded ceramic-metal matrix under harmonic excitation, J. Solid Mech., 14(3) (2024) 43-56.

[27] H. Wu, J. Zhu, S. Kitipornchai, Q. Wang, L. L. Ke, J. Yang, Large amplitude vibration of functionally graded graphene nanocomposite annular plates in thermal environments, Compos. Struct., 239 (2020) 112047.

[28] H. Wu, J. Zhu, S. Kitipornchai, Q. Wang, L. L. Ke, J. Yang, Large amplitude vibration of functionally graded graphene nanocomposite annular plates in thermal environments, Compos. Struct., 239 (2020), 112047.

[29] M. Mohammadzadeh-Keleshteri, H. Asadi, M. M. Aghdam, Geometrical nonlinear free vibration responses of FG-CNT reinforced composite annular sector plates integrated with piezoelectric layers, Compos. Struct., 171 (2017) (2017) 100-112.

[30] S. Hashemi, A. A. Jafari Nonlinear free and forced vibrations of in-plane bi-directional functionally graded rectangular plate with temperature-dependent properties, Int. J. Struct. Stab. Dyn., 20(08) (2020) 2050097.

[31] S. Hashemi, A. A. Jafari, An analytical solution for nonlinear vibration analysis of functionally graded rectangular plate in contact with fluid, Adv. Appl. Math. Mech., 13(4) (2021) 914-941.

[32] A. H. Nayfeh, D. T. Mook, Nonlinear Oscillations, WILEY-VCH Verlag & Co. KGaA, Weinheim, (2004).